the desired features and this makes the antenna suitable for both the indoor and the personal terminal WLAN and WiMAX applications. We note that its radiation pattern deteriorates slightly at the higher resonance frequency, and this may be attributed to the fact that the asymmetric ground plane of the present design is half of the CPW-fed antennas [13]. Figure 6 shows the measured peak gains of the fabricated antenna by comparing to a broadband horn antenna. The measured peak gain is about 2. 3 dBi in the lower band, while it rises slightly to approximately 2.8 dBi at the upper band. The measured peak antenna gain versus frequency varies less than 1 dBi across both operation bands.

4. CONCLUSION

In this communication, a simple ACS-fed meandered monopole antenna, with a dual-band characteristic suitable for WLAN/WiMAX application has been proposed, and has been investigated both numerically and experimentally. The use of the ACS-feed of the structure, and the coupled meandered monopole radiating elements has led to the reduction of the antenna size. It has been shown that the performance characteristics of the antenna can be modified by adjusting the dimensions of the two coupled, meandered type of monopole radiating elements, and that of the coupling gap. The antenna has the desired radiation characteristics, and impedance bandwidth, and it has a moderate gain, and these characteristics make the antenna promising for WLAN and WiMAX applications.

ACKNOWLEDGMENTS

This article is also supported by the National Nature Science Fund of China (No. 60902014 and 51209055), Nature Science Fund of Heilongjiang (QC2009C66 and ZD201115). The authors are also thankful to Hebei VSTE Science and Technology for providing the measuring facility.

REFERENCES

1. T.H. Kim and D.C. Park, Compact dual-band antenna with double L-slits for WLAN operations, IEEE Antennas Wireless Propag Lett 4 (2005), 249–252.
2. M.N. Suma, P.C. Bybi, and P. Mohanan, A wideband printed monopole antenna for 2.4GHz WLAN applications, Microwave Opt Technol Lett 48 (2006), 871–873.
3. K.G. Thomas and M. Sreenivasan, A simple dual-band microstrip-fed printed antenna for WLAN applications, IET Microwaves Antennas Propag 3 (2009), 687–694.
4. Y.F. Lin, C.H. Lin, H.M. Chen, and P.S. Hall, A miniature dielectric loaded monopole antenna for 2.4/5 GHz WLAN applications, IEEE Microwave Wireless Compon Lett 16 (2006), 591–593.
5. K.R. Rohith, M. Joseph, C.K. Aanandan, K. Vasudevan, and P. Mohanan, A new compact microstrip-fed dual-band coplanar antenna for WLAN applications, IEEE Trans Antennas Propag 54 (2006), 3755–3762.
6. C.Y. Pan, T.S. Horng, W.S. Chen, and C.H. Huang, Dual wideband printed monopole antenna for WLAN/WiMAX applications, IEEE Antennas Wireless Propag Lett 6 (2007), 149–151.
7. H.W. Liu, S.Y. Lin, and C.F. Yang, Compact Inverted-F antenna with meander shorting strip for laptop computer WLAN applications, IEEE Antennas Wireless Propag Lett 10 (2011), 540–543.
8. H. Ma, Q.X. Chu, and Q. Zhang, Compact dual-band printed monopole antenna for WLAN application, Electron Lett 44 (2008), 834–835.
9. C.Y. Huang and E.Z. Yu, A slot-monopole antenna for dual-band WLAN applications, IEEE Antennas Wireless Propag Lett 10 (2001), 500–502.
10. Y.S. Li, X.D. Yang, Y. Bai, and T. Jiang, Dual-band antenna handles WLAN/WiMAX, Microwave RF 50 (2011), 80–88.
11. Y. Seo, J. Jung, H. Lee, and Y. Lim, Design of compact dual- meander antenna for WLAN operation, Microwave Opt Technol Lett 54 (2012), 1595–1599.
12. J.H. Yoon and G.S. Kil, Compact monopole antenna with two strips and a rectangular-slit ground plane for dual-band WLAN/WiMAX applications, Microwave Opt Technol Lett 54 (2012), 1559–1566.
13. C.P. Lai, S.C. Chiu, and S.Y. Chen, Miniaturization of CPW-fed slot antennas using reactive terminations and truncated bilateral ground plane, IEEE Antennas Wireless Propag Lett 11 (2012), 1072–1075.
14. V. Deepu, R.K. Raj, M. Joseph, M.N. Suma, and P. Mohanan, Compact asymmetric coplanar strip fed monopole antenna for multiband applications, IEEE Trans Antennas Propag 55 (2007), 2351–2357.
15. V. Deepu, R. Sujith, S. Mridula, C.K. Aanandan, K. Vasudevan, and P. Mohanan, ACS fed printed F-shaped uniplanar antenna for dual band WLAN applications, Microwave Opt Technol Lett 51 (2009), 1852–1856.

V-BAND PUSH-PUSH VCO USING SLOW-WAVE CPW RESONATORS FOR LOW PHASE NOISE REDUCTION

Po-Yu Ke,[1] Hsien-Chin Chiu,[1] Fan-Hsiu Huang,[1] Hsuan-Ling Kao,[1] and Feng-Tsun Chien[2]

[1] Department of Electronics Engineering, Chang Gung University, Taoyuan, Taiwan, Republic of China; Corresponding author: hcchiu@mail.cgu.edu.tw

[2] Department of Electronics Engineering, National Chiao Tung University, Hsinchu, Taiwan

Received 7 February 2013

ABSTRACT: *This article presents a design for two fully integrated millimeter-wave V-band push–push voltage-controlled oscillators (VCOs) implemented in a 150-nm pHEMT process is presented. Both use slow-wave coplanar waveguide (CPW) structure transmission line resonators, instead of a lumped LC tank, to provide an extended output frequency range and relatively low phase noise (PN). A LC tank with and without slow-wave features is used in the two VCO circuits. The measured results for manufactured chips are compared. The VCO with the slow-wave feature demonstrates a lower PN of −104.5 dBc/Hz at a 1-MHz offset frequency. A comparison of the designs with and without a slow-wave VCO shows that the VCO design with slow wave demonstrates lower average PN of approximately 8 dBc at an offset frequency of 1 MHz. Varactor adjustment of the oscillation frequencies for the two VCOs gives 53.2 to 57.1 GHz for the VCO without slow wave and 53.8 to 55.4 GHz for the VCO with slow wave. The two VCOs are developed for use in licensed V-band transceiver systems.* © 2013 Wiley Periodicals, Inc. Microwave Opt Technol Lett 55:2373–2377, 2013; View this article online at wileyonlinelibrary.com. DOI 10.1002/mop.27827

Key words: *V-band; voltage-controlled oscillator; millimeter wave; slow-wave resonator CPW*

1. INTRODUCTION

Much effort has been expended on the development of millimeter-wave (mmW) circuits for wireless communication systems and unlicensed V-band, hence attracted tremendous attention owing to its high potential for achieving the system data rates up to Gb/s [1]. In transceiver systems, the voltage-controlled oscillator (VCO) is a key component. It provides the required local reference signal for frequency translation. Fully integrated VCO circuits are in high demand for system on-chip realization of wireless transceivers, as they provide easy and flexible integration and more reliable performance. However, at mmW frequencies, the design of such circuits is challenging

because it requires low parasitic, high-quality passives and active devices to achieve an acceptable tuning range and phase noise (PN) levels. This article describes a compact and high performance V-band GaAs pHEMT VCO that uses an electromagnetic bandgap (EBG) ground structure.

Impedance matching networks in the reported circuits use either lumped inductors [2] or EBG structure coplanar waveguide (CPW) transmission lines (T-Line) and defective ground structure (DGS) [3]. Lumped inductors offer a smaller area and larger quality factors than T-Line based matching networks, but are more difficult to precisely simulate in the mmW band. However, a modified CPW for DGS-CPW T-Lines can be considerably smaller than conventional counterparts and exhibits high Q values [2,3].

This work presents two VCOs that comply with these demands, and coverage of the license-free V-band is demonstrated in the standard 150-nm GaAs pHEMT process. A differentially slow-wave LC tank is described and a wide tuning range and low noise characteristics are achieved.

2. VCO DESIGN AND SIMULATION

2.1. Interconnecting DGS Slow CPW T-Lines

All devices presented in this article are manufactured using 150-nm GaAs technology from the WIN Semiconductor Company. The GaAs technology consists of a thin SiN layer that is deposited on a 100-μm-thick GaAs bulk substrate, as shown in Figure 1(a). The GaAs layer has a loss tangent of 0.001 and a dielectric constant of 12.9. The multilayer is formed in steps: first, a 1-μm-thick layer is deposited and then a 2-μm-thick layer is deposited. One of the two metal layers is on top of layer 1 and the other is between the two SiN layers. The choice of the technology used in filter design depends on the desired selectivity. Figure 1(b) shows the slow-wave CPW (S-CPW) topology, which consists of a classical CPW T-Line that is loaded by DGS. In this study, Metal-1 is the DGS S-CPW topology, which is composed of a classical CPW T-Line, on which is loaded a ground patterned metalic shield (Metal-1). The gap G between the CPW and the ground patterned metallic shield strips is then adjusted to achieve the required characteristic impedances.

Figure 1(b) shows the circuit layout of the proposed S-CPW, using DGS. In a conventional CPW, grounded microstrip T-Lines on GaAs typically exhibit a quality factor in V-band applications of the order of 5–15, which is not sufficient for filter and T- Line design. As the slow-wave T-Line has been shown to provide much higher Q values [2], this is chosen. Figure 1(b) shows the structure of the slow-wave T-Lines that are utilized in this work. The slotted bottom metalic shields are

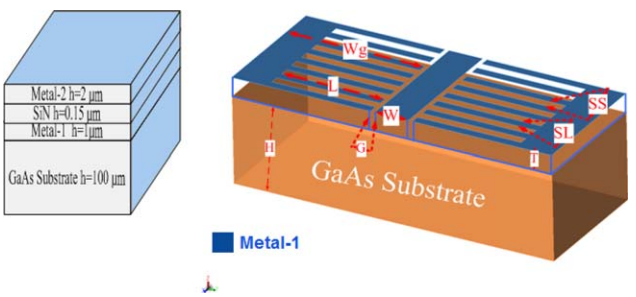

Figure 1 (a) The stack of the 0.15 InGaAs technology from the WIN Semiconductor Company. (b) A three-dimensional view of the S-CPW topology. [Color figure can be viewed in the online issue, which is available at wileyonlinelibrary.com]

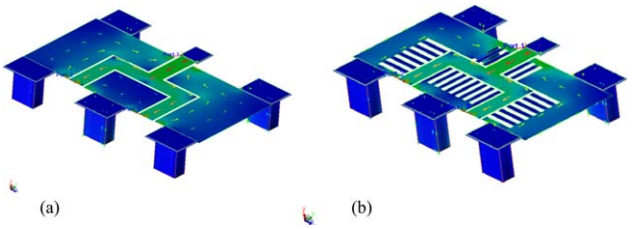

Figure 2 (a) Structure of the standard CPW T-Lines and (b) the DGS S-CPW T-Lines. [Color figure can be viewed in the online issue, which is available at wileyonlinelibrary.com]

patterned with 130 μm-long (L) metal stripes that are separated by slots with a width of 10 μm (SS = SL). The width of the signal line metal is 37 μm (W), the distance between the signal line metal and the metallic ground is 5 μm (G), the length of the signal line is 450 μm (L-T-Line) and the ground plane is 250 μm (Wg). The resistivity of each metal layer is 0.02 Ω/square and the insulator layer is GaAs.

The electromagnetic simulation of DGS T-Lines is fairly complex, but can be preformed successfully. The numerical analysis of the DGS S-CPW VCO studied uses the commercial computer software package, Momentum, of Agilent Technologies, Advanced Design System, which uses the method of moment technique for layered media. Momentum solves mixed potential integral equations using full wave Green's functions.

The EM simulation of the DGS S-CPW T-Lines is fairly complex, but it can be performed successfully. Figures 2(a) and 2(b) compare the standard CPW T-Lines and the DGS S-CPW T-Lines. Figure 3 shows the simulated performance of the T-Line. High Q values are obtained.

2.2. Design of the DGS Slow-Wave CPW VCO

The compound VCO based GaAs have high f_t and f_{max}, low substrate loss and high-Q on-chip transmission line, and passive components. Figure 4 shows an LC-tank push–push VCO with a cross-coupled differential pair, Ml and M2. Two varactors, C_t, are used for tuning and a combination of different drain outputs is used to minimize the load to the oscillator core and to allow 50-Ω output matching. The two VCOs presented use the same circuit topology, but different transmission line resonant inductors, one having a slow-wave feature and the other not having a slow-wave structure.

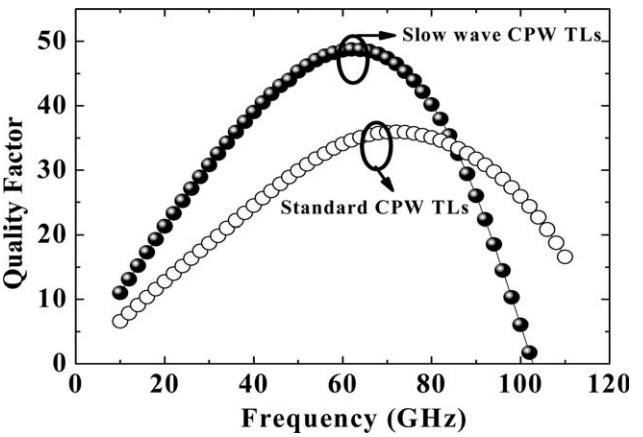

Figure 3 Simulated quality factor

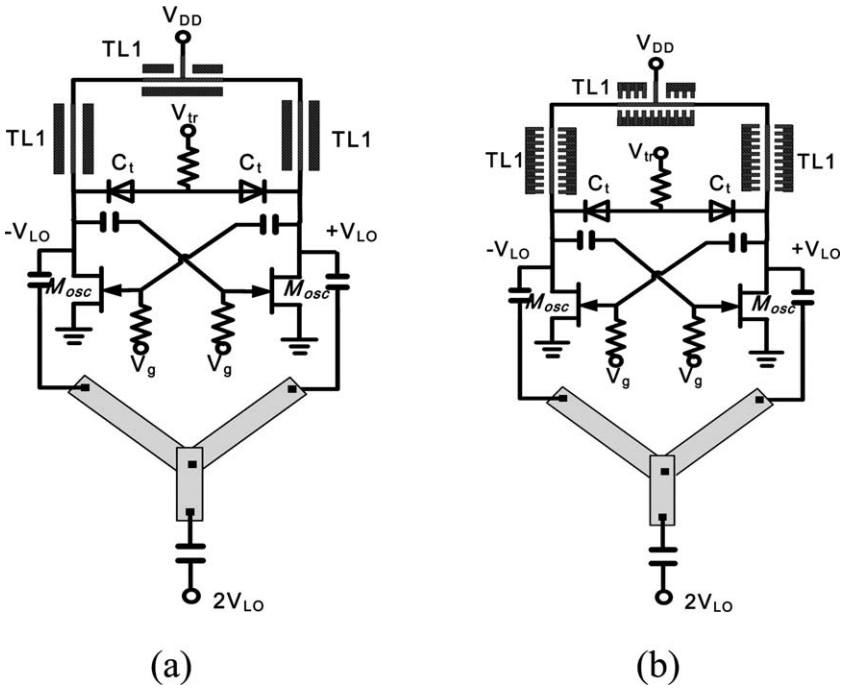

Figure 4 Circuit schematic of the designed V-band push–push VCOs (a) LC-tank without slow-wave VCO and (b) LC-tank with slow-wave VCO

$$\Delta\omega = \frac{1}{\sqrt{L_{\tan k}[(C_{t\max} - C_{t\min}) + C_{\tan k}]}} \tag{1}$$

where

$$L_{\tan k} = 3TL_1 C_{\tan k} = 2C_{gs} + 2C_{ds} + 2C_c \tag{2}$$

C_t is the varactor capacitance, $C_{\tan\ k}$ is the capacitance of the oscillator transistor, M_{osc}, and C_c is the capacitance of the RF DC block. The subscript *gs* indicates the gate to source and *ds* the drain to source. Equation (1) uses a linear time-invariant approximation for the oscillation frequency of an LC-tank push–push VCO, so it neglects the nonlinearity of the varactor tuning curve and various small-signal parasitic effects. Equation (1) can only be used for initial design estimation. The classical distribution of $L_{\text{total}}\{\Delta\omega\}$ into phase and amplitude fractions assumes an equal division of noise, so that Eq. (3) [4]

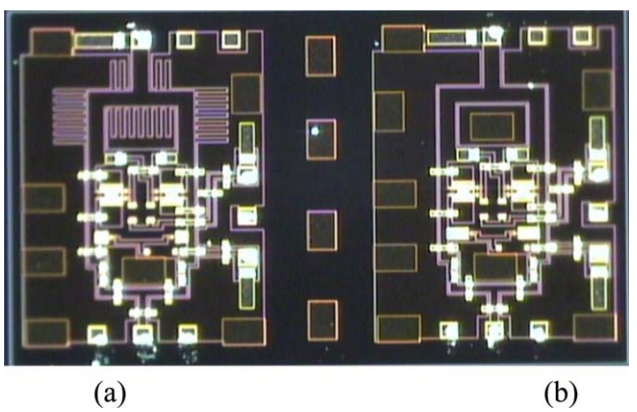

Figure 5 The chip micrographs for (a) LC-tank with slow-wave VCO and (b) LC-tank without slow-wave VCO. [Color figure can be viewed in the online issue, which is available at wileyonlinelibrary.com]

$$L_{\text{phase}}\{\Delta\omega\} = L\{\Delta\omega\} = L_{\text{total}}\{\Delta\omega\}/2 \tag{3}$$

$$L(\Delta\omega)P \propto \frac{(\text{gm}/I)\Gamma V_{\text{DD}}}{Q_{\text{T}}^2} \cdot \left(\frac{\omega_0}{\Delta\omega}\right)^2 \tag{4}$$

Equation (4) also illustrates the importance of the quality factor of the tank circuit. A high tank quality factor results in low noise and power-efficient oscillators. However, the quality factor is dependent on the technology available for the fabrication of the tank and is mostly beyond the control of a circuit designer. The specification, constraints, design variables, and design relationships for the oscillator are summarized in Figure 4. The design uses appropriate values for L, C, Γ, and transistor size (gm/I) so that the center frequency ω_0 and the start-up and PN requirement $L\{\Delta\omega\}$ meet the requirements, with the lowest possible power consumption, P.

3. VCO DESIGN AND SIMULATION

The two push–push VCOs are manufactured on a 150-nm commercial GaAs chip with two metal layers. The differential CPW tank is constructed on Metal-1 and the slow-wave ground is constructed on Metal-1. The on-chip lumped capacitor is integrated in each VCO chip one for the dc ground and two for the dc blocks at the two differential outputs. The chip micrographs are shown in Figure 5. The size of each integrated VCO circuit is approximately 0.78×0.61 mm^2.

An Agilent E4446A 3 MHz to 44 GHz spectrum analyzer was used to measure the VCO output spectrum and the tuning range. An Agilent 11970U mixer was used to characterize and measure the VCO PN. Figure 6 shows the measured VCO output spectrum with the control voltage set at 0 V. The slow-wave tank VCO has a center resonator frequency of 55.17 GHz, whereas this value is 56.31 GHz for the tank VCO without slow wave. Slow-wave ground loads the capacitance to the CPW transmission line, thereby lowering the oscillator frequency. Figure 7 shows the measurements for the PN. This figure shows that the measured PN in the slow-wave tank VCO is -104 dB/

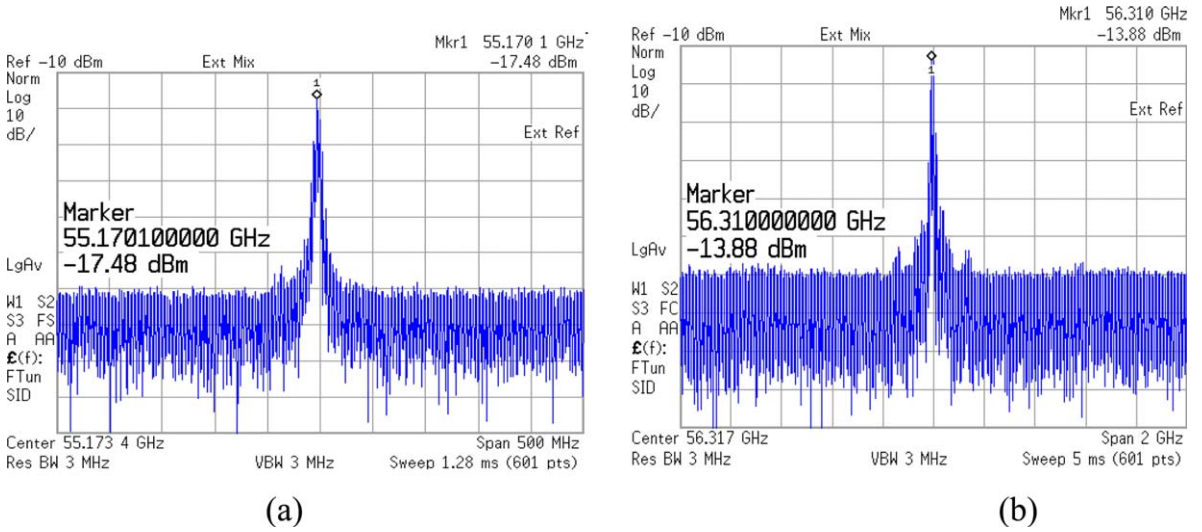

Figure 6 Measured VCO output spectrum (a) LC-tank with slow-wave VCO and (b) LC-tank without slow-wave VCO. [Color figure can be viewed in the online issue, which is available at wileyonlinelibrary.com]

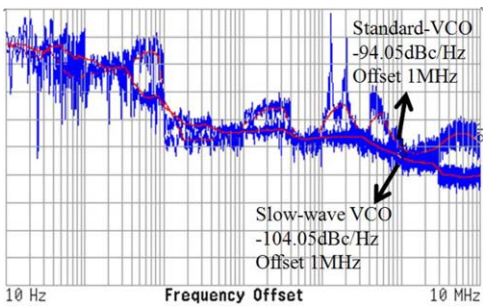

Figure 7 Measurement of the PN. [Color figure can be viewed in the online issue, which is available at wileyonlinelibrary.com]

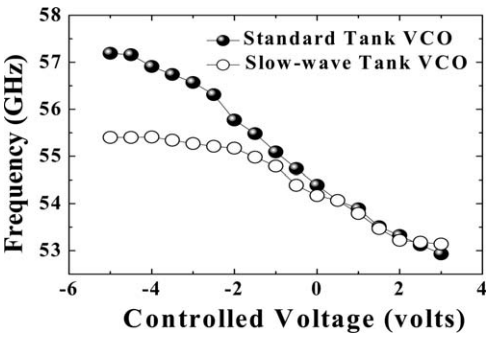

Figure 8 Measured VCO tuning range

Hz at an offset frequency of 1 MHz. The slow-wave VCO exhibits an average 8-dBc improvement over a standard tank VCO at offset frequencies from 100 Hz to 10 MHz. However, both VCOs have a similar oscillation frequency and output-power characteristics. Figure 8 shows the oscillation frequencies for both VCOs, which are 53.8 to 55.4 GHz for slow-wave tank VCO and 53.2 to 57.1 GHz for the standard tank VCO, at voltages from −5 to 1 V. In high output power mode, the total power consumption of the VCO, including buffers, is 42 mW, from a 3 V supply. Table 1 compares the performance of the VCOs in the V-band.

4. CONCLUSION

This research shows that CPW transmission-line-based LC-tank resonators can improve the performance of mmW VCOs. The proposed slow-wave tank VCO has a lower PN of −104 dBc/Hz at an offset frequency of 1 MHz, which represents a 9 dBc improvement over the standard-VCO. The measurement results show that this slow-wave based GaAs VCO has great potential for high-frequency and low-PN oscillator applications. Varactor adjustment of the oscillation frequencies for two VCOs gives 53.2 to 57.1 GHz for the VCO without slow wave and 53.8 to 55.4 GHz for the VCO with slow wave. The two VCOs are suitable for use in licensed V-band transceiver systems.

ACKNOWLEDGMENTS

The authors wish to thank the facilities support from High Speed Intelligent Communication (HSIC) Research Center,

TABLE 1 Comparison with Published V-band VCOs

Ref.	Tech.	Center Freq. (GHz)	Tuning Range (GHz)	Phase Noise (1-MHz Offset dBc/Hz)	Power (mW)
[5]	0.18-μm CMOS	52	0.6	−97	27
[6]	90-nm CMOS	58.4	5.4	−91.2	8.1
[7]	65-nm CMOS	60	10.2	−97.1	30
[8]	0.11-μm pHEMT	59.7	04	−86	NA
This work (standard)	0.15-μm pHEMT	56.3	1.6	−94.05	42
This work (slow wave)	0.15-μm pHEMT	55.1	3.9	−104.05	42

Healthy Aging Research Center (HARC) in Chang Gung University and National Nano Device Laboratories, Taiwan.

REFERENCES

1. S.E. Gunnarsson et al., 60 GHz single-chip front-end MMICs and systems for multi-Gb/s wireless communication, IEEE J Solid-State Circuits 42 (2007), 1143–1157.
2. F. Yang, K. Ma, Y. Qian, and T. Itoh, A uniplanar compact photonic bandgap (DC-PBG) structure and its applications for microwave circuits, IEEE Trans Microwave Theory Tech 47 (1999), 1509–1514.
3. H.B. El-Shaarawy, F. Coccetti, R. Plana, M. EI-Said, and E.A. Hashish, Compact bandpass ring resonator filter with enhanced wide-band rejection characteristics using defected ground structures, IEEE Microwave Wireless Compon Lett 18 (2007), 500–503.
4. W. Robins, Phase noise in signal sources (theory and applications), IEE Telecommunications Series, Peter Peregrinus Ltd, UK, 1982..
5. Y.H. Cho, M.D. Tsai, H.Y. Chang, C.C. Chang, and H. Wang, A low phase noise 52 GHz push-push VCO in 0.18 um bulk CMOS technologies, In: IEEE Radio Frequency Integrated Circuit Conference, Long Beach, CA, June 2005, pp. 131–134.
6. L. Li et al., Design and analysis of a 90 nm mm-waveoscillator using inductive-division LC tank, IEEE J Solid-State Circuits 44 (2009), 1950–1958.
7. B. Cath and M. Hella, A 60 GHz CMOS combined mm-waveVCO/divider with 10-GHz tuning range, In: IEEE CICC Digest, September 2009, pp. 669–672.
8. Y. Kawasaki, K. Shirikawa, Y. Ohashi, and T. Saito, 60 GHz monolithic oscillator using InGaP/InGaAs/GaAs HEMT technology, In: IEEE MTT-S Digest, Orlando, FL, Vol. 2, May 1995, pp. 541–544.

A SOLAR-POWERED 2.4-GHz LNA RFIC

Jian-Ming Wu and Yan-Tsang Lin
Department of Electronic Engineering, National Kaohsiung Normal University, No. 62, Shenjhong Rd., Kaohsiung 824, Taiwan, Republic of China; Corresponding author: jianmingwu@nknucc.nknu.edu.tw

Received 8 February 2013

ABSTRACT: *A 2.4-GHz low-noise amplifier (LNA) radio frequency integrated circuit is designed and implemented using the 18-μm CMOS standard process for ZigBee applications. A solar panel with a regulator circuit directly converts solar power to the electrical power of the LNA. The forward body bias method is applied to reduce the power consumed by the LNA, as required to provide green energy. Measurements of the solar-powered 2.4-GHz LNA are made, revealing that the noise figure is 2.91 dB, the gain is 10.89 dB, and the input-referred third-order intercept point is 0 dBm. A voltage of 0.6 V is supplied to the LNA and the power consumption is then 1.08 mW.* © 2013 Wiley Periodicals, Inc. Microwave Opt Technol Lett 55:2377–2380, 2013; View this article online at wileyonlinelibrary.com. DOI 10.1002/mop.27823

Key words: *low-noise amplifier; solar power; forward body bias; low power*

1. INTRODUCTION

The ZigBee Alliance announced the development of the ZigBee PRO Green Power in December 2012. In ZigBee PRO Green Power, a highly efficient energy harvesting method is utilized to collect energy from the ambient environment, including solar energy, RF radiation energy, mechanical energy, human energy, thermal energy, wind energy, and other forms. Then, the harvested energy is converted to electrical energy, which supplies the radio frequency integrated circuits (RFICs) in ZigBee systems. In the literature, most of the electricity that is used by self-powered RFICs is RF radiation energy [1–4]. The solar-powered RFIC has been seldom discussed.

Green considerations require that an RF receiver must consume low power. The first stage of an RF receiver is a low-noise amplifier (LNA), which amplifies an RF signal. As an LNA is a critical component of an RF receiver system, reducing its power consumption (P_{DC}) can greatly reduce the total power consumption of the receiver. Several approaches for designing a low-power LNA have been presented. They are included: (1) the forward body bias technique [5–8]; (2) the folded cascade technique [9]; and (3) the current reuse technique [10,11]. The forward body bias method is simple to implement, but has the leakage current of body-source junctions. The folded cascade method provides favorable isolation, but it is complicated in design. The drop in power consumption that is associated with the current reuse technique is high, but a high supply voltage is required.

The purpose of this work is to design and implement a 2.4-GHz LNA using the TSMC 0.18-μm CMOS standard process for ZigBee systems. Notably, a solar panel with a regulator circuit directly transforms solar power to the electrical power of the LNA. The simple forward body bias technique is used to reduce the power consumed by the LNA, as required to provide green energy.

2. A SOLAR PANEL WITH A REGULATOR

The sun is inexhaustible and its energy is easy to obtain from the environment. Solar energy can be collected and converted into electricity using solar panels, which exploit the photovoltaic effect. Figure 1 presents a monocrystalline silicon solar panel with an area of 12.5×4 cm^2. Highly intense sunlight, such as seen at noon, produces a large dc output power of the solar panel. A regulator is required to protect the LNA from damage when the solar panel generates and supplies electrical power to the LNA.

Figure 2 shows the regulator circuit. The LM317L, which is manufactured by Fairchild Semiconductor, is utilized as a voltage regulator. The resistors R_1 and R_2 provide the output voltage of LM317L. Capacitor C_1 is a filter capacitor. Capacitor C_2 improves transient responses. The lowest output voltage of LM317L is 1.2 V. Therefore, the voltage divider that is composed of resistors R_3 and R_4 provides 0.6 V, which is the supply voltage of the LNA.

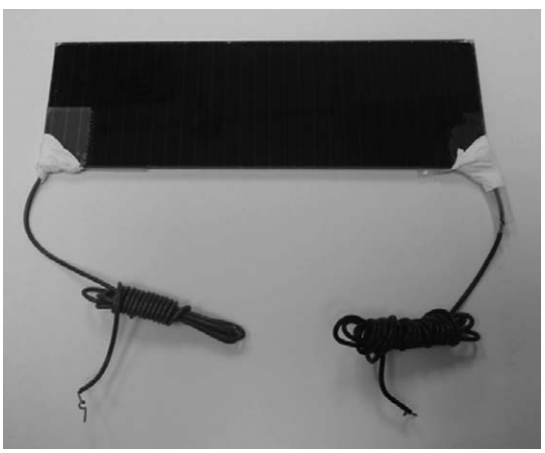

Figure 1 Monocrystalline silicon solar panel